

See discussions, stats, and author profiles for this publication at: <https://www.researchgate.net/publication/285177434>

Barotropic tides in channelized estuaries

Article · January 2010

DOI: 10.1017/CBO9780511676567.004

CITATIONS
138

READS
1,175

1 author:



Carl Friedrichs
Virginia Institute of Marine Science
183 PUBLICATIONS 8,974 CITATIONS

[SEE PROFILE](#)

Barotropic tides in channelized estuaries

CARL T. FRIEDRICH S

Virginia Institute of Marine Science, College of William and Mary

3.1. Introduction

This chapter addresses the dynamics of cross-sectionally averaged tidal currents and elevation in channelized estuaries. The tides considered here are further assumed to be entirely barotropic and externally forced. Given these constraints, a series of estuarine geometries are examined which attempt to encompass generic, reasonably realistic scenarios found in nature. Typically, the goal in each case is to determine the lowest-order physical balances governing barotropic tides for a realistically relevant geometry, derive an analytical expression for the speed of tidal phase propagation, solve for the amplitude and phase of tidal velocity relative to that of elevation, and determine the lowest-order variation in tidal amplitude with distance along the estuary. A few less realistic, but classically studied cases (e.g., those involving an intermediate length, constant width channel) are also considered for completeness. For most cases, examples of estuaries that reasonably represent and justify the simplified dynamics are discussed.

In this chapter we generally assume that tidal elevation (η) and cross-sectionally averaged tidal velocity (u) along an estuary can be described at lowest order by

$$\eta(x, t) = a(x) \cos(\omega t - kx), \quad u(x, t) = U(x) \cos(\omega t - kx - \phi), \quad (3.1a,b)$$

where x is along-channel distance (positive into the estuary), t is time, a and U are tidal elevation and velocity amplitude, ω and k are tidal frequency and wavenumber, and ϕ is the relative phase between tidal elevation and velocity. Tidal frequency and wavenumber, in turn, are defined as $\omega = 2\pi/T$ and $k = 2\pi/\lambda$, where T and λ are the tidal period and wavelength. Note that equation (3.1) represents the tide as a forward-propagating, variable-amplitude wave without the explicit presence of a reflected wave. This approach is consistent with the manner in which observations of spatial variations in tidal phase, kx , are typically reported with distance along real estuaries. By using a formulation more-or-less consistent with commonly reported

observations, observed variations in amplitude and phase can more easily be used to directly scale the governing equations.

The next three sections of this chapter present and then scale the governing equations of mass and momentum conservation. An essential step in this process is the identification of key length scales, corresponding inverse length scales (or “spatial rates of change”), and dimensionless ratios to be used subsequently to determine when and where to keep or neglect various dynamic or kinematic terms. Sections 3.5 through 3.14 then examine specific estuary geometries (e.g., short vs long, shallow vs deep, funnel-shaped vs non-convergent) that allow simplifications to be made. These simplifications are particularly relevant to better understanding fundamental physics in real tidal estuaries. The order of presentation proceeds from cases that are dynamically the most simple, yet still observationally useful, toward somewhat more complicated but naturally common “equilibrium” and “near-equilibrium” estuaries. Along the way, controls on tidal asymmetries are specifically considered in the context of short and/or shallow estuaries. For completeness, non-equilibrium channels and reflected wave cases are also briefly considered. Channels with lateral variations in bathymetry are considered in Chapter 6.

Themes emphasized in this chapter include the following: (i) it is valuable to use observations to scale the governing equations applicable to a tidal estuary in order to better understand the dominant physics and, in the process, avoid applying an overly complex and/or incorrect analytical framework; (ii) a unidirectional, up-estuary propagating waveform is applicable to a wide variety of long-channel geometries; (iii) the relative phase between tidal velocity and elevation can be shown to be close to “standing” ($\sim 90^\circ$) in many short and/or shallow estuaries without the need to explicitly include a classical reflected wave; (iv) there is a morphodynamic tendency for the amplitude of tidal velocity to vary along-estuary less dramatically than width and/or tidal phase; (v) variation in tidal amplitude and phase speed along such systems results when the net effects of width convergence and bottom friction do not quite balance; (vi) the total width of a tidal estuary (including tidal storage in marsh, shoals, and/or tidal tributaries) can play an important role in slowing the rate of up-estuary tidal wave propagation; and (vii) tidal variations in system width or channel depth can result in a shorter high- or low-water slack, shorter falling or rising tidal elevation, and stronger ebb or flood currents.

Several papers over the last two decades have presented generalized analytical solutions for cross-sectionally averaged barotropic tides in a wide range of estuarine geometries that include channel convergence (Jay, 1991; Friedrichs and Aubrey, 1994; Friedrichs *et al.*, 1998; Lanzoni and Seminara, 1998; Prandle, 2003, 2004; Savenije and Veling, 2005; Savenije *et al.*, 2008). These series of papers demonstrate the growing awareness among theoreticians that tidal amplitude, phase speed, and the relative phase between tidal velocity and elevation in most river valley

estuaries are largely controlled by a competition between bottom friction and channel convergence. In addition, variations in tidal velocity amplitude along morphologically active, tidally energetic estuaries tend to be relatively small, and prominent reflected waves are uncommon. However, these advances in theoretical understanding have remained somewhat hidden from non-specialists by the formal mathematical analysis and presentation style of some authors.

This chapter, which is based on class lecture notes designed for non-specialists, aims to present a similar story as the above references, but in the most straightforward manner possible – while still retaining essential analytical components. For example, equations and variables are not non-dimensionalized here, and intuitive symbols are chosen wherever possible (e.g., L for length scales, A for areas, w for widths, etc.). Step-by-step approaches for scaling the governing equations and deriving analytical solutions are explicitly presented, and the series of cases considered starts with the simplest first. (More formal analyses often start out with more complete but possibly opaque solutions, followed by specific asymptotes.) Furthermore, the majority of the theoretical cases considered here are motivated and justified by clear observational analogues in order to ground theoretical insights in applied reality.

3.2. Governing equations

The generic estuarine geometry of interest to this chapter is shown in Fig. 3.1. The estuary is assumed to be channelized such that $w(x)$ is the width of the portion within which all along-estuary transport of mass and momentum is assumed to reside (e.g., Friedrichs and Aubrey, 1988). The tidally varying (but width-averaged) depth of the channelized portion is given by $h(x,t)$; $b(x,t) \geq w(x)$ is the tidally varying width of the estuary as a whole (including fringing marsh and shoals, intertidal flats and, potentially, smaller tidal tributaries); and x follows the possibly curving axis of flow along the main channel.

The cross-sectionally integrated conservation of mass (or “continuity”) equation for barotropic tides is then given by

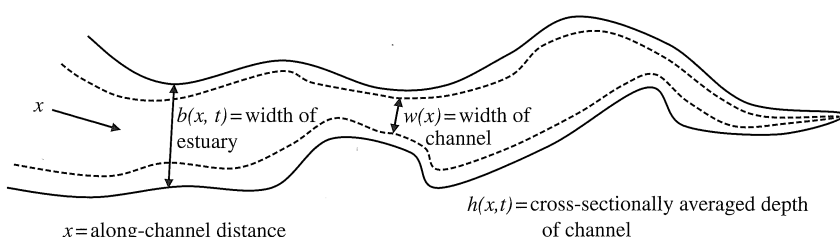


Figure 3.1. Generic tidal estuary plan-view geometry.

$$b \frac{\partial \eta}{\partial t} = - \frac{\partial}{\partial x} (uwh) \quad (3.2)$$

(e.g., Ippen and Harleman, 1966). The left-hand side (l.h.s.) of equation (3.2) represents the time rate of change in the wetted cross-sectional area of the estuary (including intertidal storage areas), while the right-hand side (r.h.s.) represents along-channel convergence in volume flux within the channel alone. It is assumed that there is negligible along-channel flow over areas outside the channelized portion of the estuary.

The cross-sectionally averaged tidal momentum equation is given approximately by

$$\frac{\partial u}{\partial t} + u \frac{\partial u}{\partial x} + g \frac{\partial \eta}{\partial x} + \frac{\tau_b}{\rho h} = 0 \quad (3.3)$$

(e.g., Ippen and Harleman, 1966), where g is gravitational acceleration, τ_b is bottom stress averaged over the channel perimeter, and ρ is water density. The terms in equation (3.3), from left to right, are local acceleration, advective acceleration, along-channel pressure gradient, and bottom friction. The above formulation neglects minor errors in $u \partial u / \partial x$ associated with averaging over the cross-section. However, it will soon be shown that the entire $u \partial u / \partial x$ term does not affect lowest-order solutions for a , U , or tidal propagation in the channelized systems of most interest to this chapter.

3.3. Scaling momentum

Our first step in simplifying and scaling the momentum equation is to linearize the friction term as follows:

$$\frac{\tau_b}{\rho h} = \frac{1}{\rho h} (\rho c_d u |u|) = ru \left[1 \pm O\left(\frac{a}{\langle h \rangle} \pm \frac{8}{15\pi}\right) \right], \quad (3.4)$$

where “ $O()$ ” indicates “order of”, and the two leading terms in the Fourier expansion arise from tidal variations in h and from linearizing $u|u|$ (Parker, 1991). In equation (3.4), the bottom drag coefficient c_d is on the order of 10^{-2} to 10^{-3} (depending on the roughness scale),

$$r = \frac{c_d}{\langle h \rangle} \frac{8U}{3\pi} \quad (3.5)$$

is the friction factor, and $\langle \rangle$ indicates a tidal average.

The next step is to substitute equations (3.4) and (3.5) into equation (3.3) and eliminate u and η in equation (3.3) using equation (3.1). For the purpose of evaluating the order of magnitude of the various terms in equation (3.3), after

performing differentiations, we set $\sin(\)$ and $\cos(\)$ equal to 1. The momentum equation in terms of scales then becomes:

$$\begin{aligned} & \pm O(\omega U) \pm O[U(L_U^{-1}U \pm kU)] \pm O[g(L_a^{-1}a \pm ka)] \\ & \pm O\left[rU\left(1 \pm \frac{a}{\langle h \rangle} \pm \frac{8}{15\pi}\right)\right] = 0. \end{aligned} \quad (3.6)$$

Note that $\partial u / \partial x$ and $\partial \eta / \partial x$ in equation (3.3) each produce two terms in equation (3.6) because u and η are potentially dependent on x in two distinct ways: (i) x -dependence of the tidal amplitudes (via $\partial U / \partial x$ and $\partial a / \partial x$); (ii) phase-dependence of u and η (via $\partial(kx) / \partial x$). L_U^{-1} and L_a^{-1} in equation (3.6) are scales (with units of 1/km) for the spatial rates of change of tidal velocity and elevation along the channel – i.e., L_U^{-1} and L_a^{-1} scale the size of $\partial / \partial x$ in $\partial U / \partial x$ and $\partial a / \partial x$, respectively. Said another way, their inverses, L_U and L_a , are the characteristic along-channel distances over which U and a vary. L_U^{-1} and L_a^{-1} are formally defined as

$$L_U^{-1} = \frac{\partial U / \partial x}{U}, \quad L_a^{-1} = \frac{\partial a / \partial x}{a}. \quad (3.7a, b)$$

At first, the definitions in equation (3.7) may appear to be somewhat circular. But we will see that the magnitudes L_U^{-1} and L_a^{-1} can often be evaluated a priori directly from data (via observed e-folding lengths, for example), which aids in the process of appropriately simplifying equations (3.2) and (3.3) for application to real estuaries.

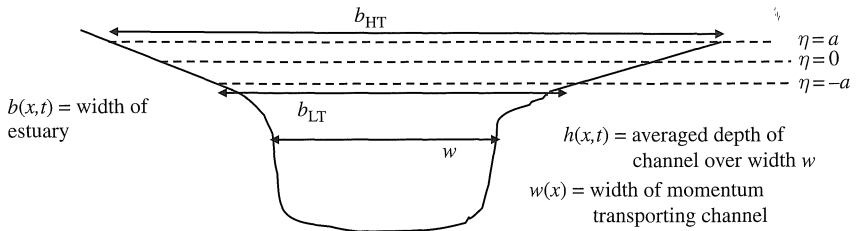
Dividing the terms in equation (3.6) by ωU , we see that the maximum size of the friction term relative to local acceleration (to leading order) is r/ω , and the maximum size of the advective term relative to $\partial u / \partial t$ is given by $(U/c)(1 + (kL_U)^{-1})$, where $c = \omega/k$ is the phase velocity of the tidal waveform. In mildly non-linear systems, we anticipate that U/c will usually be much less than 1. Thus we expect that advection will only be important where tidal velocity amplitude U changes dramatically over very short along-channel distances (i.e., if L_U^{-1} is very large).

3.4. Scaling continuity

In some shallow estuaries of interest, the total estuary width b varies significantly in time due to the presence of extensive intertidal flats and/or marsh (Fig. 3.2). Under these conditions, scaling the l.h.s. of equation (3.2) yields:

$$b \frac{\partial \eta}{\partial t} = \langle b \rangle \left[1 \pm O\left(\frac{\Delta b}{\langle b \rangle}\right) \right] \frac{\partial \eta}{\partial t}, \quad (3.8)$$

where Δb is the amplitude of estuary width variation over the tidal cycle.



$$\Delta b = \text{amplitude of tidal estuary width change} = (b_{HT} - b_{LT})/2$$

Figure 3.2. Generic tidal estuary cross-section geometry.

Expanding $\partial/\partial x$ on the r.h.s. of equation (3.2) while accounting for tidal variations in channel depth yields:

$$-\frac{\partial}{\partial x}(uwh) = -uw \langle h \rangle \left(\frac{1}{u} \frac{\partial u}{\partial x} + \frac{1}{w} \frac{\partial w}{\partial x} + \frac{1}{\langle h \rangle} \frac{\partial \langle h \rangle}{\partial x} \right) \left[1 \pm O\left(\frac{a}{\langle h \rangle}\right) \right]. \quad (3.9)$$

Balancing equations (3.8) and (3.9), applying the definitions of η and u , differentiating, and further scaling then gives:

$$\begin{aligned} \omega a \langle b \rangle & \left[1 \pm O\left(\frac{\Delta b}{\langle b \rangle}\right) \pm O\left(\frac{a}{\langle h \rangle}\right) \right] \\ & = uw \langle h \rangle k O \left[1 \pm \frac{L_U^{-1}}{k} \pm \frac{L_w^{-1}}{k} \pm \frac{L_h^{-1}}{k} \right], \end{aligned} \quad (3.10)$$

where

$$L_w^{-1} = \frac{\partial w / \partial x}{w}, \quad L_h^{-1} = \frac{\partial \langle h \rangle / \partial x}{\langle h \rangle} \quad (3.11a,b)$$

are the spatial rates of change in channel width and depth.

The mass balance represented by equation (3.10) is between the time rate of change of the wetted cross-sectional area on the l.h.s. and along-channel convergence of volume flux on the r.h.s. At leading order, flux convergence on the r.h.s. is due to the sum of (i) the along-channel rate of change in the phase of tidal velocity ($\sim \partial(kx)/\partial x \approx k$), (ii) the along-channel rate of change in the amplitude of tidal velocity (which scales as L_U^{-1}), (iii) the along-channel rate of change in channel width ($\sim L_w^{-1}$), and (iv) the along-channel rate of change in channel depth ($\sim L_h^{-1}$). To non-dimensionalize the r.h.s. of equation (3.10), these four terms have all been divided by k . Table 3.1 summarizes the key ratios of temporal and spatial scales (or, in many cases, ratios of spatial rates of change) used to evaluate the importance of the various terms in the momentum and continuity equations.

Table 3.1. Ratios used to evaluate the importance of terms and likely size of approximation errors in the momentum and continuity equations (in order of appearance in text)

Ratio	Compact form used in text (if different)	Definition
$\frac{a}{\langle h \rangle}$	—	$\frac{\text{amplitude of tidal elevation}}{\text{average channel depth}}$
$\frac{r}{\omega}$	—	$\frac{\text{magnitude of friction term in momentum}}{\text{magnitude of acceleration term in momentum}}$
$\frac{U}{c}$	—	$\frac{\text{tidal velocity amplitude}}{\text{tidal phase speed}}$
$\frac{L_U^{-1}}{k}$	$(kL_U)^{-1}$	$\frac{\text{spatial rate of change in } U}{\text{spatial rate of change in tidal phase}}$
$\frac{\Delta b}{\langle b \rangle}$	—	$\frac{\text{amplitude of tidal variation in estuary width}}{\text{average estuary width}}$
$\frac{L_w^{-1}}{k}$	$(kL_w)^{-1}$	$\frac{\text{spatial rate of change in channel width } w}{\text{spatial rate of change in tidal phase}}$
$\frac{L_h^{-1}}{k}$	$(kL_h)^{-1}$	$\frac{\text{spatial rate of change in } h}{\text{spatial rate of change in tidal phase}}$
$\frac{L}{k^{-1}}$	kL	$\frac{\text{length of estuary}}{\text{length scale over which tidal phase varies}}$
$\frac{L}{L_a}$	—	$\frac{\text{length of estuary}}{\text{length scale for along-channel variation in } a}$
$\frac{k}{L_w^{-1}}$	kL_w	$\frac{\text{spatial rate of change in tidal phase}}{\text{spatial rate of change in } w}$
$\frac{L_h^{-1}}{L_w^{-1}}$	L_w/L_h	$\frac{\text{spatial rate of change in } h}{\text{spatial rate of change in } w}$
$\frac{L_U^{-1}}{L_w^{-1}}$	L_w/L_U	$\frac{\text{spatial rate of change in } U}{\text{spatial rate of change in } w}$
$\frac{ L_w^{-1} - L_b^{-1} }{L_w^{-1}}$	$ L_w - L_b /L_b$	$\frac{\text{difference between spatial rates of change in } w \text{ and } b}{\text{spatial rate of change in } w}$
$\frac{\omega}{r}$	—	$\frac{\text{magnitude of acceleration term in momentum}}{\text{magnitude of friction term in momentum}}$
$\frac{L_a^{-1}}{k}$	$(kL_a)^{-1}$	$\frac{\text{spatial rate of change in tidal amplitude}}{\text{spatial rate of change in tidal phase}}$

3.5. Short estuaries

In short tidal estuaries, it is possible to integrate continuity from an arbitrary location x to the head at L in order to solve directly for tidal velocity without considering momentum. Performing a leading-term Taylor expansion on $\partial\eta/\partial t$ and integrating both sides of equation (3.2) in x yields:

$$\frac{\partial\eta_0}{\partial t} \left[1 \pm O\left(kL \pm \frac{L}{L_a}\right) \right] \int_x^L b \, dx = -[(uwh)_L - (uwh)_x], \quad (3.12)$$

where L is the length of the estuary, and η_0 is tidal elevation at the mouth of the estuary (at $x = 0$).

Assuming no tidal flux at the landward end of the estuary, $(uwh)_L = 0$, and a short tidal estuary ($kL \ll 1$, $L/L_a \ll 1$), equation (3.12) reduces to

$$u(x, t) = \frac{\partial\eta_0(t)}{\partial t} \frac{A_b(x, t)}{A_c(x, t)}, \quad (3.13)$$

where $A_c = wh$ is the wetted channel cross-sectional area at x , and $A_b = \int b \, dx$ is the wetted basin surface area up-estuary of x .

The expected errors in equation (3.13) of size $O(kL, L/L_a)$ are only negligible if the estuary is indeed very short. But equation (3.13) is otherwise fully non-linear, and the solution for $u(x, t)$ given by equation (3.13) can be calculated based just on a knowledge of intertidal topography, local channel bathymetry, and a time series of tidal elevation at a single point. At a given point in x , tidal variations in A_b/A_c can lead to significant distortion in $u(t)$, as illustrated in Fig. 3.3. If h increases dramatically over the tidal cycle, but b does not, the resulting velocity–stage curve will display higher velocities around low water (Fig. 3.3a–b). Conversely, if b changes more strongly than h , higher velocities will be found in the tidal channel around high water (Fig. 3.3c–d). In short estuaries, the momentum equation is inconsequential to the calculation of $u(x, t)$, and tidal phase speed, c , is effectively infinite, since zero phase lag is assumed along the length of the system.

Linearizing equation (3.13) leads to the solution:

$$\eta(t) = a_0 \cos \omega t, \quad u(x, t) = -U(x) \sin \omega t, \quad U(x) = a_0 \omega < A_b(x) / A_c(x) >, \quad (3.14a-c)$$

with additional errors $O(a < h >, \Delta b < b >)$. From equation (3.14) it follows that in short estuaries, the linearized component of tidal velocity is 90° out of phase with tidal elevation. Although this is the same phase relation found in a tidal standing wave, it was not necessary to evoke a reflected wave or momentum in any form to derive this result.

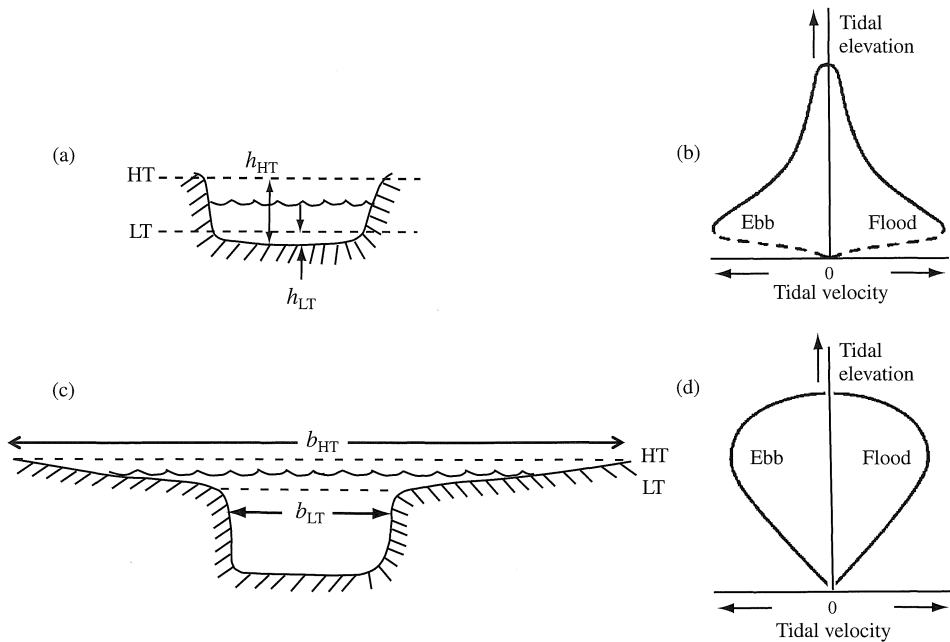


Figure 3.3. (a) Tidal estuary dominated by tidal variations in channel depth. (b) Tidal currents in the channel are strongest closer to low tide when depth is small. (c) Tidal estuary dominated by tidal variations in estuary width. (d) Tidal currents in the channel are strongest closer to high tide when surface area is large. [(b), (d) adapted from Pethick, 1980.]

The short estuary case approximated by equation (3.13) is discussed at length by Pethick (1980). Real-world examples include channelized tidal marsh, mangrove and tidal flat systems, a few kilometers or less in length, found ubiquitously on coastlines around the globe. Specific systems from the literature explicitly examined in the context of the above dynamics include tidal channels near Wachapreague, Virginia, as discussed by Boon (1975), and tidal channels near North Norfolk, England, as discussed by Pethick (1980).

3.6. Long, shallow, funnel-shaped estuaries

A second class of tidal estuaries characterized by a simple solution for tidal velocity that follows directly from continuity are shallow, funnel-shaped estuaries. Figure 3.4 displays along-channel variation in a , kx , $\langle A_c \rangle$, $\langle b \rangle$, and U as observed along the Tamar, Delaware, and Thames estuaries (from Friedrichs and Aubrey, 1994). Values for L_a , L_{Ac} , L_b , L_h , L_w , and L_U (based on exponential fits), and k (based on a linear fit) are contained in Table 3.2. From Table 3.2, we see that the largest term

Table 3.2. Observed tidal and geometric properties for example funnel-shaped estuaries (from Friedrichs and Aubrey, 1994). Values are along-channel averages or otherwise apply to the estuary as a whole. Because low-water elevation in the upper Tamar is kinematically truncated around low water, parameters derived from $a(x)$ and kx along the Tamar are based on the elevation of high water

Parameter	Tamar	Thames	Delaware
a (m)	2.7	2.0	0.64
$\langle h \rangle$ (m)	2.9	8.5	5.8
L (km)	21	95	215
k (1/km)	1/64	1/70	1/58
L_w^{-1} (1/km)	1/5.8	1/18	1/40
L_b^{-1} (1/km)	1/4.6	1/25	1/40
L_{Ac}^{-1} (1/km)	1/5.3	1/19	1/38
$ L_h^{-1} $ (1/km)	1/62	1/72	1/720
$ L_a^{-1} $ (1/km)	1/190	1/1500	1/570
$ L_U^{-1} $ (1/km)	1/160	1/280	1/1700
$\frac{L_w^{-1}}{k}$	11	3.9	1.45
$\left \frac{L_h^{-1}}{k} \right $	1.0	1.0	0.08
$\left \frac{L_U^{-1}}{k} \right $	0.40	0.25	0.03
$a/\langle h \rangle$	0.94	0.24	0.11
$\Delta b/\langle b \rangle$	0.29	0.17	~ 0
$w/\langle b \rangle$	0.71	0.83	~ 1

on the r.h.s. of equation (3.10) for this class of estuary is $(kL_w)^{-1}$. Assuming $w \sim \exp(-x/L_w)$ and $b \sim \exp(-x/L_b)$, such that $L_w \approx L_b$, the lowest-order, linearized continuity balance becomes

$$\frac{\partial \eta}{\partial t} = \frac{w \langle h \rangle L_w^{-1}}{\langle b \rangle} u, \quad (3.15)$$

with associated errors $O(kL_w, L_w/L_h, L_w/L_U, |L_w - L_b|/L_b, a/\langle h \rangle, \Delta b/\langle b \rangle)$. Note that the above errors are not necessarily negligible (e.g., $a/\langle h \rangle$ in the Tamar, kL_w in the Delaware). Nonetheless, the largest linear terms in each case lead to the above simple balance, effectively highlighting fundamental physics. The effects of additional terms on tidal asymmetry and along-channel changes in tidal amplitude will be discussed in detail in later sections.

Plugging equation (3.1) into equation (3.15) immediately gives the solution

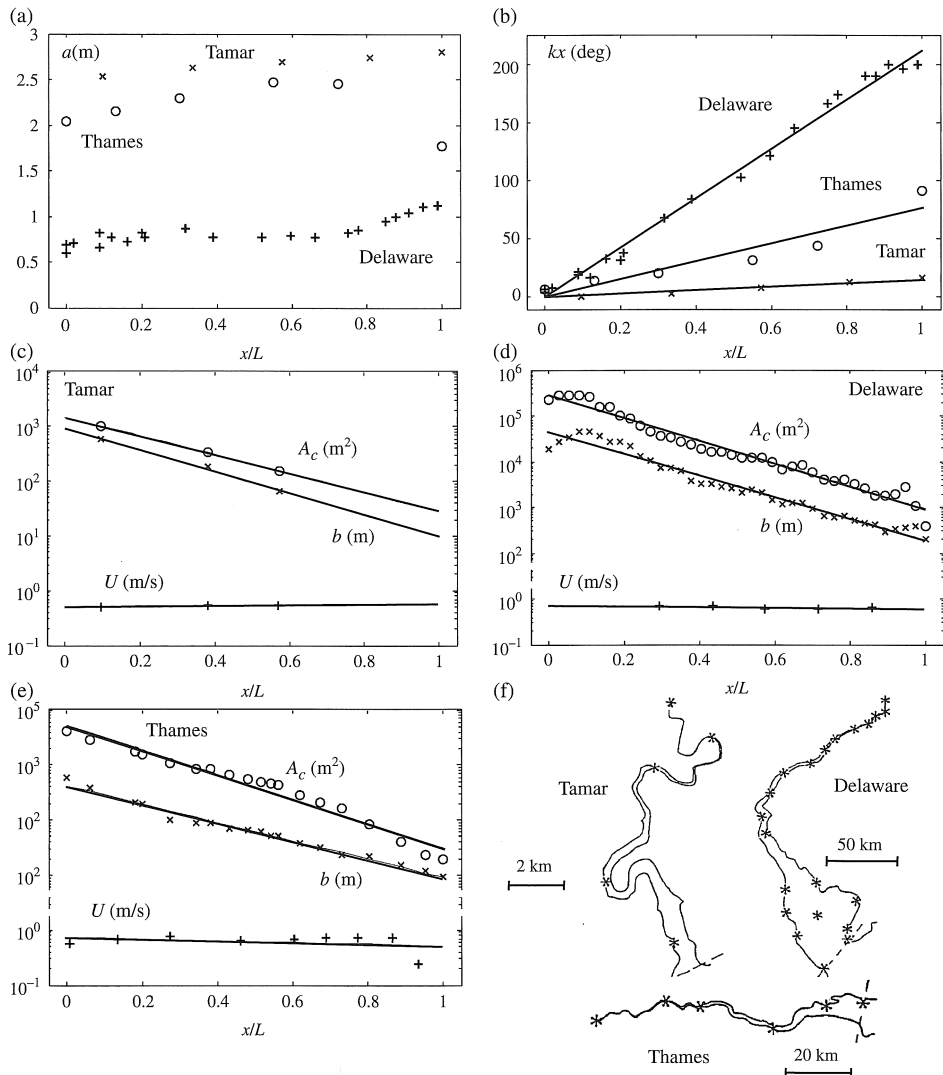


Figure 3.4. Along-estuary variation in: (a) tidal elevation amplitude (\times Tamar, \circ Thames, $+$ Delaware); (b) tidal phase (\times Tamar, \circ Thames, $+$ Delaware); channel cross-sectional area (\circ), estuary width (\times), tidal velocity amplitude ($+$) for (c) Tamar, (d) Delaware; (e) Thames; (f) tide gauge locations. Adapted from Friedrichs and Aubrey (1994).

$$\eta(t) = a \cos(\omega t - kx), \quad u(x, t) = -U \sin(\omega t - kx),$$

$$U = \frac{a\omega \langle b \rangle}{\langle h \rangle L_w^{-1} w}. \quad (3.16a-c)$$

As was the case for short channels, we are here likewise able to solve for the magnitude and phase of tidal velocity relative to elevation based on externally

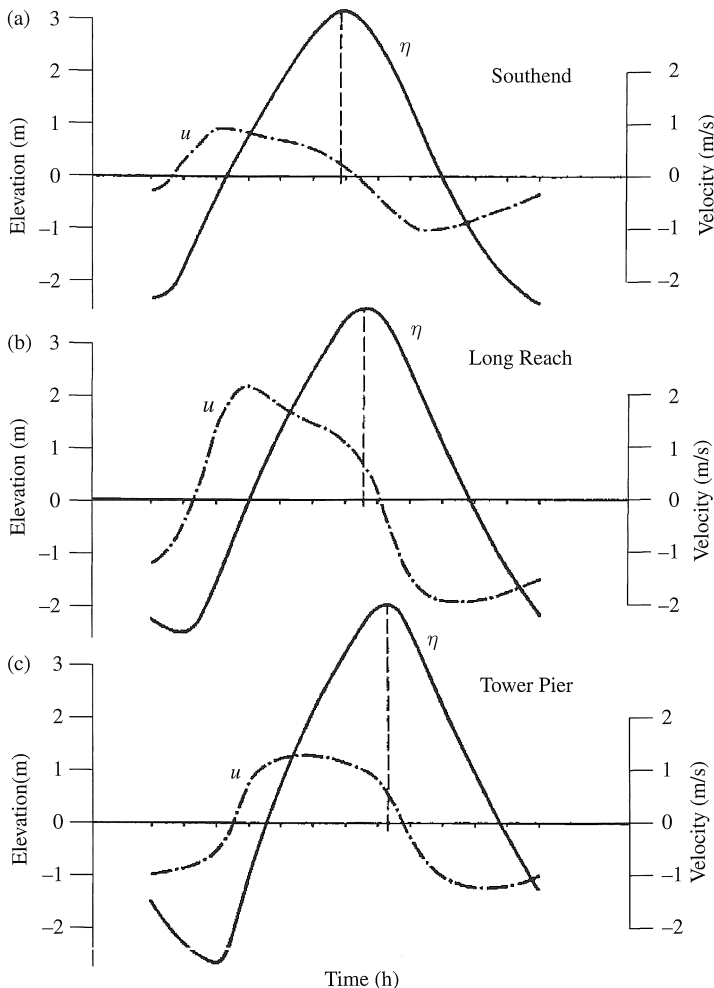


Figure 3.5. Observed tidal elevation and cross-sectionally averaged velocity curves for 11 February 1948 measured (a) 0.2, (b) 13, and (c) 27 km downstream from London Bridge. Note that velocity leads tidal elevation with a relative phase of $\sim 90^\circ$. Adapted from Hunt (1964).

imposed variables (a , ω , b , w , L_m , h) without evoking momentum. Equation (3.16), like equation (3.14) above, indicates that velocity leads elevation by 90° , as in a classic standing wave. This result is consistent with the relationship between tidal velocity and elevation illustrated by observations from the Thames in Fig. 3.5. Yet kx in Fig. 3.4b clearly indicates that the associated waveform propagates landward. This contradiction reiterates the potential confusion that may result if an estuary as a whole is characterized as having a “standing” or “progressive” wave character based only on the phase relationship between velocity and elevation.

The linearized momentum equation resulting from scaling in Section 3.3 is:

$$\frac{\partial u}{\partial t} + g \frac{\partial \eta}{\partial x} + ru = 0. \quad (3.17)$$

Plugging the known solution given by equation (3.16) into equation (3.17), however, results in no terms available to balance $\partial u / \partial t$. This imbalance can only be neglected at lowest order if ω/r is also a small parameter. Thus we have the interesting result that if width changes dominate along channel changes in depth, velocity amplitude, and tidal phase, it must follow that friction dominates acceleration, even though we do not explicitly know anything about what the bed roughness is.

Equation (3.17) is then approximated as:

$$g \frac{\partial \eta}{\partial x} + ru = 0. \quad (3.18)$$

Combining equations (3.15) and (3.18) to eliminate u then yields:

$$\frac{\partial \eta}{\partial t} + c \frac{\partial \eta}{\partial x} = 0, \quad (3.19)$$

where the tidal phase speed c in equation (3.19) is given by

$$c = \frac{\omega}{k} = \frac{g \langle h \rangle_w L_w^{-1}}{r \langle b \rangle}. \quad (3.20)$$

The wave speed in equation (3.20) increases with depth, $\langle h \rangle$, and with increased channel convergence (i.e., larger L_w^{-1}). Conversely, wave speed decreases with greater friction, r , and with greater tidal volume storage in fringing shoals, flats and marsh (i.e., larger $\langle b \rangle/w$).

Equation (3.19) is an example of a first-order wave equation (termed “first-order” because $\partial/\partial t$ and $\partial/\partial x$ are first derivatives). A first-order wave equation allows propagation of waves in only one direction, in this case up-estuary toward $+x$. Reflected waves (which propagate toward $-x$) are not allowed. Physically, reflected waves do not occur in this type of system because waves propagating toward $-x$ have their energy quickly spread by divergence of width as well as being damped by friction. Waves propagating toward $+x$ are frictionally damped too, but convergence concentrates wave energy enough to maintain a relatively constant amplitude of tidal velocity and elevation.

3.7. Long, deep, non-convergent estuaries

As an example of (an approximately) long, deep and non-convergent estuary channel, we will take the main stem of the 300-km long Chesapeake Bay. From Fig. 3.6, the spatial rate of change in tidal phase in Chesapeake Bay is approximately

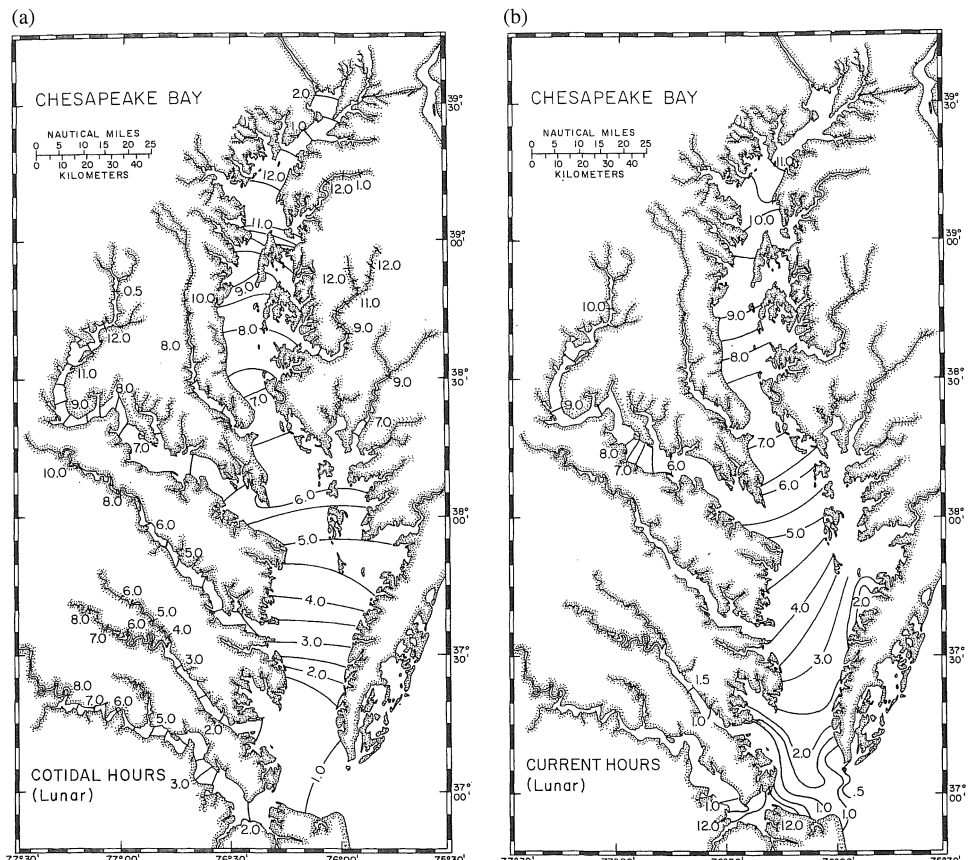


Figure 3.6. Tidal phase in hours for (a) high tide and (b) maximum flood current along the Chesapeake Bay and its major tidal tributaries (from Carter and Pritchard, 1988).

$k \approx 1/(50 \text{ km})$ for the semidiurnal tide. From equation (3.10), we then see that as long as spatial rates of change in U , w , and h are all much greater than $1/(50 \text{ km})$, then phase-induced changes in volume flux dominate the r.h.s. of the equation. In other words, if the e-folding lengths of U , w , and h are much greater than 50 km (which they are), then the lowest-order, linearized continuity balance must be between the $\partial\eta/\partial t$ and $\partial(kx)/\partial x$ terms. Plugging equation (3.1) into these two remaining terms immediately yields:

$$\eta(x, t) = a \cos(\omega t - kx), \quad u(x, t) = U \cos(\omega t - kx), \quad U = \frac{a\omega \langle b \rangle}{\langle h \rangle kw}. \quad (3.21a-c)$$

The above solution shows that in long, deep, constant-width tidal channels, velocity and elevation are in phase. Figure 3.6 shows that η and u are indeed largely in phase

over most of the main stem of the Chesapeake Bay, except within about 100 km of the head, where a reflected wave is indicated by a shift in the velocity–elevation phase difference from ~ 0 to ~ 3 hours at the very top of the bay.

This time, plugging the solution given by equation (3.21) into equation (3.17) results in no terms available to balance the friction term ru . In a manner analogous yet opposite to that presented in Section 3.6, this imbalance can only be neglected if r/ω is a small parameter no larger than $O(kL_w)^{-1}$. Thus, we now have the result that if (i) the spatial rate of change in tidal phase (k) dominates the spatial rates of change in width (L_w^{-1}), depth (L_h^{-1}), and velocity amplitude (L_U^{-1}), then (ii) it must follow that acceleration dominates friction ($r/\omega \ll 1$) in the momentum transporting channel, even though we still do not have (or need) an explicit measure of bottom roughness.

Assuming a momentum balance between the $\partial u / \partial t$ and the $\partial(kx) / \partial x$ component of pressure gradient, a continuity balance between $\partial \eta / \partial t$ and the $\partial(kx) / \partial x$ component of flux convergence, and cross-differentiating to eliminate u then yields:

$$\frac{\partial^2 \eta}{\partial t^2} - c^2 \frac{\partial^2 \eta}{\partial x^2} = 0, \quad c = \frac{\omega}{k} = \left(\frac{g \langle h \rangle w}{\langle b \rangle} \right)^{1/2}. \quad (3.22a,b)$$

Equation (3.22a) is a second-order wave equation, which allows propagation of waves in both $+x$ and $-x$. Physically, reflected waves can occur in this type of system (at least for a finite distance) because a relatively small rate of channel width change and low friction does not cause immediate divergence or dissipation of reflected energy. For the case of $w = \langle b \rangle$ (i.e., negligible tidal storage outside the central channel), equation (3.22b) reduces to $c = (g \langle h \rangle)^{1/2}$, the familiar solution for a frictionless, non-convergent, shallow-water wave. However, the presence of inter-tidal areas, lateral shoals, and/or other areas of tidal storage often slows tidal propagation in real estuaries.

We can check the assumption of low channel friction in the main stem of the Chesapeake Bay as follows. With $k \approx 1/(50 \text{ km})$ and $a \approx 0.25 \text{ m}$, equations (3.21c) and (3.22b) can be combined to give $U \approx 35 \text{ cm/s}$. Based on a high-resolution numerical model, Spitz and Klinck (1998) suggest a median value of $c_d \approx 0.001$ for the Chesapeake. Assuming the channelized portion of the Chesapeake Bay (not including shallow lateral shoals) to have a mean depth of about $\langle h \rangle \approx O(10 \text{ m})$, it then follows from equation (3.5) that $r \approx 3 \times 10^{-5} \text{ s}^{-1}$. The magnitude of friction relative to local acceleration, r/ω , is then 0.2, which is indeed small at our order of accuracy.

It is interesting to note that assuming $w = b$ in equation (3.22) would result in an unrealistic solution for tidal propagation in the Chesapeake Bay. Based on Fig. 3.6, the phase speed for the tide in the Chesapeake Bay is about 7 m/s. Neglecting lateral tidal storage areas by applying $c = (g \langle h \rangle)^{1/2}$ would then give

$\langle h \rangle = 5$ m. However, the mean depth of the Chesapeake Bay is significantly larger at 8.5 m (NOAA, 1985). The simplest explanation is that tidal volume storage in lateral shoals and tidal tributaries slows tidal propagation up the bay as predicted by equation (3.22b).

3.8. Long, shallow, non-convergent estuaries

For the case of long, shallow, non-convergent estuaries, friction dominates acceleration in momentum, and along-channel gradients in tidal velocity dominate along-channel variations in width and depth. The linearized governing equations are then

$$g \frac{\partial \eta}{\partial x} + ru = 0, \quad \langle b \rangle \frac{\partial \eta}{\partial t} = -w \langle h \rangle \frac{\partial u}{\partial x}, \quad (3.23a,b)$$

with errors $O(\omega/r, (kL_w)^{-1}, (kL_h)^{-1}, a/\langle h \rangle, \Delta b/\langle b \rangle)$. The above balances can be a useful approximation when exploring the dynamics of shallow tidal channels with abundant fringing marsh and/or tidal flats for which the short estuary assumption is not justifiable (Friedrichs and Madsen, 1992).

Differentiating equation (3.23a) in order to eliminate u in equation (3.23b) gives

$$\frac{\partial \eta}{\partial t} = D \frac{\partial^2 \eta}{\partial x^2}, \quad D = \frac{wg \langle h \rangle}{\langle b \rangle r}. \quad (3.24a,b)$$

Equation (3.24) has the form of a diffusion equation with the coefficient D describing the upstream evolution of the tidal signal. With the boundary conditions that $\eta = a_0 \cos(\omega t)$ at $x = 0$ and $\eta \rightarrow 0$ as $x \rightarrow \infty$ (i.e., $kL \gg 1$), the solution to equation (3.24) is then

$$\eta(x, t) = a_0 \exp(-kx) \cos(\omega t - kx), \quad c = \frac{\omega}{k} = \left(\frac{2\omega g \langle h \rangle w}{r \langle b \rangle} \right)^{1/2}. \quad (3.25a,b)$$

Plugging equation (3.25a) into equation (3.23a) then yields

$$u(x, t) = U_0 \exp(-kx) \cos(\omega t - kx + \pi/4), \\ U_0 = \frac{a_0}{\langle h \rangle} \left(\frac{\omega g \langle h \rangle \langle b \rangle}{rw} \right)^{1/2}. \quad (3.26a,b)$$

The relative phase between elevation and velocity in equation (3.25) and equation (3.26) is $\phi = -\pi/4$. In other words, velocity leads elevation by 45° , and the relationship between η and u is intermediate between standing and progressive. However, the partially “standing” behavior has nothing to do with reflection, since there is no reflected wave.

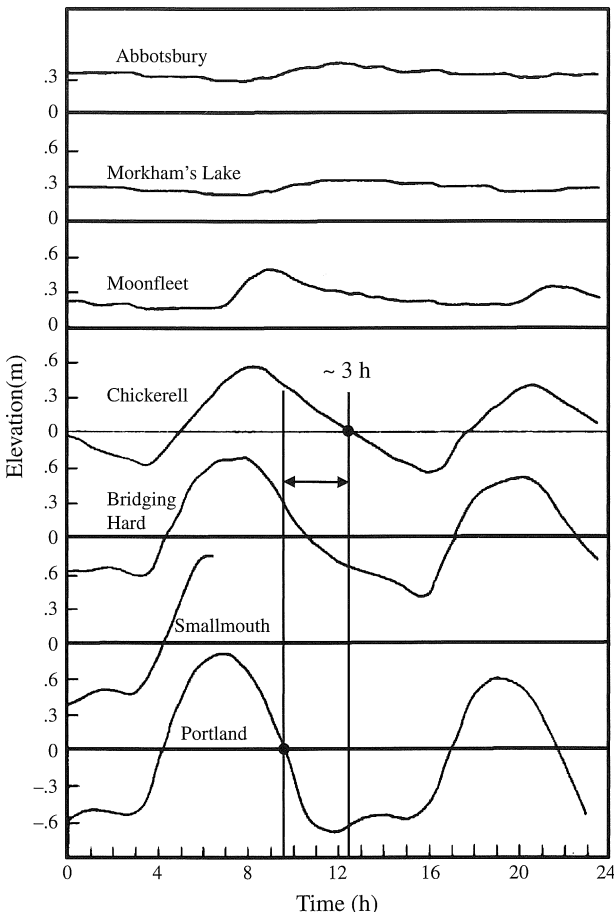


Figure 3.7. Observed tidal elevations along The Fleet during spring tide, 17 December 1967, collected 0, 0.3, 2, 5, 7, 11, and 13 km up-estuary of Portland. Adapted from Robinson *et al.* (1983).

As a real-world example, we take The Fleet, a very shallow, relatively long and straight back-barrier lagoon lined with tidal marsh, located along the south coast of England (Fig. 3.7). From Robinson *et al.* (1983), for The Fleet we have $\langle h \rangle = 0.7$ m, $\langle b \rangle = 390$ m, $w = 130$ m, $a_0 = 0.7$ m, and estuary length $L = 13$ km. From Fig. 3.7 we see that $c \approx 0.5$ m/s, so from equation (3.25b) we can derive that $\omega/r = 0.05$, confirming that frictional dominance is a good approximation in this case. For the semidiurnal tide, $c \approx 0.5$ m/s gives $k \approx 1/(3 \text{ km})$, confirming that $kL \ll 1$ and the estuary can be treated as infinitely long. It is interesting to note that Robinson *et al.* (1983) recognized the important role storage in fringing marshes can play in slowing tidal propagation. But they applied the

frictionless phase speed given by equation (3.22b) to The Fleet rather than the frictionally dominated solution given by equation (3.25b).

3.9. Tidal asymmetry in shallow estuaries

Linearizing continuity and momentum yields errors of size $O(a/\langle h \rangle, \Delta b/\langle b \rangle)$. Accounting for the decay of $a(x)$ along The Fleet, the average value for $a/\langle h \rangle$ in our real-world example is about 0.7. Thus, one might expect significant non-linear distortion of the tidal wave as it propagates along the estuary. In Fig. 3.8, one can see that the rising tide in The Fleet does indeed become shorter relative to the falling tide with distance landward. The cause of this asymmetry can be understood conceptually by examining the behavior of the tidal phase speed as a function of changes in estuary width and depth.

Substituting the definition for r back into equation (3.25b) for shallow, non-convergent estuaries yields

$$c = \left(\frac{3\pi\omega w g \langle h \rangle^2}{4c_d U \langle b \rangle} \right)^{1/2}. \quad (3.27)$$

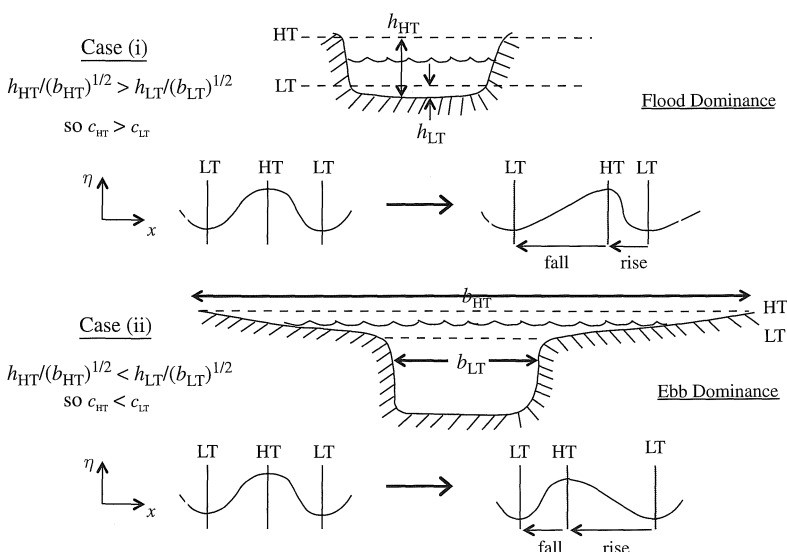


Figure 3.8. (i) In a tidal estuary dominated by tidal variations in channel depth, high tide propagates faster, partially catching up with the previous low tide. The result is a shorter rising tide and flood dominance. (ii) In a tidal estuary dominated by tidal variations in estuary width, low tide propagates faster, partially catching up with the previous high tide. The result is a shorter falling tide and ebb dominance.

The above equation is a linearized solution for wave speed, so c in equation (3.27) is assumed to be constant in time. A non-linear perturbation analysis (following Friedrichs and Madsen, 1992) yields a similar but time-dependent relationship such that

$$c(t) \sim h(t)/[b(t)]^{1/2}, \quad (3.28)$$

allowing c to vary in time at $O(a/\langle h \rangle, \Delta b/\langle b \rangle)$. Based on the time-dependent form in equation (3.28), at times when the tidal channel is deeper or the wetted estuary cross-section is narrower (relative to the width of the main channel), the tidal signal will propagate faster; when the channel is shallower or the estuary wider, the tidal signal will propagate more slowly. A qualitatively similar relationship results if one applies this analysis to equation (3.20) for shallow, funnel-shaped estuaries, namely $c \sim h^2/b$.

In other words (and as further represented in Fig. 3.8), if the channel is much deeper around high tide than around low tide ($h_{HT} \gg h_{LT}$), high tide will propagate into the estuary faster. High water will partially “catch up” with the previous low tide, and the duration of the rising tide will be shorter. Conversely, if the estuary is much wider at high tide than at low tide ($b_{HT} \gg b_{LT}$), low tide will propagate into the estuary faster, low tide will partially “catch up” with the previous high tide, and the duration of the falling tide will be shorter.

A leading-term Taylor expansion of $h/b^{1/2}$ over the tidal cycle gives

$$c \sim \frac{h}{b^{1/2}} \approx \frac{\langle h \rangle [1 + (\eta/a)(a/\langle h \rangle)]}{\langle b \rangle^{1/2} [1 + (\eta/a)(\Delta b/\langle b \rangle)]^{1/2}} \approx \frac{\langle h \rangle}{\langle b \rangle^{1/2}} [1 + \gamma(\eta/a)], \quad (3.29)$$

where

$$\gamma = \frac{a}{\langle h \rangle} - \frac{1}{2} \frac{\Delta b}{\langle b \rangle} \quad (3.30)$$

is a tidal asymmetry parameter (cf. Friedrichs and Madsen, 1992). If $\gamma > 0$, tidal changes in depth dominate changes in width, and the tide is faster rising. If $\gamma < 0$, changes in width dominate, and the tide is faster falling. Because the phase of tidal velocity relative to elevation is at least partially standing in the frictionally dominated estuaries described by equations (3.29) and (3.30), these systems will tend to be flooding during the rising tide and ebbing during the falling tide. For these cases, $\gamma > 0$ corresponds to a faster rising tide and therefore flood dominance, while $\gamma < 0$ corresponds to a faster falling tide and therefore ebb dominance.

In order to investigate the role of channel depth and intertidal storage in determining flood vs ebb dominance, Friedrichs and Aubrey (1988) solved equations (3.2) and (3.3) numerically, retaining all non-linearities including quadratic friction. They considered 84 combinations of channel depth and total estuarine

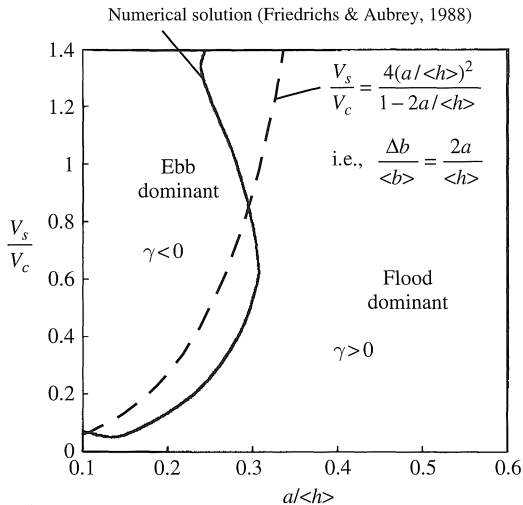


Figure 3.9. Regions of ebb and flood dominance as a function of tidal amplitude to channel depth ratio ($a/\langle h \rangle$) and volume of storage in intertidal areas relative to volume of channels (V_s/V_c). $\Delta b/\langle b \rangle$ is the amplitude of estuary width change over the tidal cycle divided by tidally-averaged estuarine width. The two lines separating the ebb- and flood-dominant fields are non-linear numerical results from Friedrichs and Aubrey (1988) (solid line) and equation (3.31) (dashed line).

width, all with $L = 7$ km, $c_d = 0.01$, $w \approx 100 \langle h \rangle$, $a_0 = 0.75$ m, and linearly sloping intertidal flats. In each case, w , $\langle h \rangle$, and $\langle b \rangle$ were uniform along-channel. Based on an intuitive scaling rather than equations (3.28)–(3.30), Friedrichs and Aubrey (1988) suggested the two governing parameters to be $a/\langle h \rangle$ and V_s/V_c , where V_s is the volume of storage in intertidal areas at high tide, and V_c is the volume in subtidal channels at mean water. Figure 3.9 displays the regions in V_s/V_c and $a/\langle h \rangle$ “space” that Friedrichs and Aubrey (1988) found to be flood and ebb dominant, respectively.

The theoretical line separating flood- and ebb-dominant systems can alternatively be found by setting $\gamma = 0$ in equation (3.32), i.e., the situation where $\Delta b/\langle b \rangle = 2a/\langle h \rangle$. (Note that the very same relationship ends up separating flood- and ebb-dominant cases for shallow, funnel-shaped systems.) Using our present notation, $V_s/V_c \approx (2a\Delta b)/[h(\langle b \rangle - \Delta b)]$ for cases where $w \approx b$ at low tide (like those modeled by Friedrichs and Aubrey, 1988). Setting $\Delta b/\langle b \rangle = 2a/\langle h \rangle$ then gives the analytical curve shown in Fig. 3.9, where $\gamma = 0$, namely

$$\frac{V_s}{V_c} = \frac{4(a/\langle h \rangle)^2}{1 - 2a/\langle h \rangle} . \quad (3.31)$$

Both equations (3.30) and (3.31) indicate that for $2a/\langle h \rangle \geq 0.5$, there is no amount of intertidal area or storage volume that can overcome depth-dependence and induce a faster-falling tide. Furthermore, the plot of equation (3.31) superimposed on Fig. 3.9 shows that the simple approximation given by equations (3.29) and (3.30) reasonably reproduces the fully non-linear results of Friedrichs and Aubrey (1988).

3.10. Tides in long, intermediate-depth, equilibrium estuaries

We now generalize the cases from Sections 3.6 and 3.7, i.e., long estuaries that maintain nearly uniform tidal amplitude along the length of the estuary. We term this generalized type of weakly to strongly funnel-shaped estuary an “equilibrium” estuary because uniform tidal velocity amplitude in space is associated with morphodynamic equilibrium (e.g., Friedrichs, 1995). The simplest approach in terms of mathematical analysis is to look for a solution that is the real part of the following (with $i = (-1)^{1/2}$):

$$\eta(x, t) = a \exp [i(\omega t - kx)] , \quad u(x, t) = U \exp [i(\omega t - kx - \phi)] , \quad (3.32a,b)$$

and assume that at least one of k or L_w^{-1} is $\gg L_h^{-1}$ and L_U^{-1} . We will also assume $a/\langle h \rangle \ll 1$, $\Delta b/\langle b \rangle \ll 1$, and $w \sim b \sim \exp(-x/L_w)$. However, we now allow $(kL_w)^{-1} = O(1)$ and $r/\omega = O(1)$.

Plugging equation (3.32) into equations (3.2) and (3.17) with the above assumptions gives the following for continuity and momentum:

$$i\omega ab = ikwhUe^{-i\phi} + whUL_w^{-1}e^{-i\phi}, \quad i\omega Ue^{-i\phi} - ikga + rUe^{-i\phi} = 0, \quad (3.33a,b)$$

where h and b are still tidally averaged, but we have dropped the brackets for brevity. [Note that it follows from equation (3.33a) that $L_a^{-1} \approx L_U^{-1}$.] Equations (3.33a) and (3.33b) can then be rearranged respectively to become

$$\frac{\omega a}{U} e^{i\phi} = -\frac{kwh}{b} + \frac{iwhL_w^{-1}}{b}, \quad \frac{\omega a}{U} e^{i\phi} = -\frac{\omega^2}{kg} + \frac{i\omega r}{kg} = 0. \quad (3.34a,b)$$

By separately equating the real and imaginary parts of equations (3.34a) and (3.34b), it immediately follows that

$$c = \frac{\omega}{k} = \left(\frac{ghw}{b} \right)^{1/2} \quad \text{and} \quad c = \frac{\omega}{k} = \frac{ghwL_w^{-1}}{rb}. \quad (3.35a,b)$$

In other words, in equilibrium estuaries, the phase-speed relationships for deep, straight estuaries and shallow, funnel-shaped estuaries hold simultaneously. The fact

that $c \approx (gh)^{1/2}$ in such systems (for cases where $b \approx w$) has likely caused confusion in the past. In an equilibrium estuary, the frictionless wave speed holds regardless of the relative importance of friction (cf. Hunt, 1964). But this definitely does not mean the dynamic balance associated with a frictionless wave applies.

Furthermore, by eliminating either ghw/b or ω/k in equation (3.35), we have the added constraints that

$$\frac{r}{\omega} = \frac{L_w^{-1}}{k}, \quad \text{and} \quad L_w = \frac{(ghw/b)^{1/2}}{r}. \quad (3.36a,b)$$

The equality of r/ω and $(kL_w)^{-1}$ in equation (3.36a) emphasizes the balance between the effects of friction and convergence in equilibrium estuaries. As friction becomes more important (as indicated by a greater r/ω), width convergence must similarly strengthen [i.e., $(kL_w)^{-1}$ must increase] in order to maintain tidal amplitude. The near equality of $(kL_w)^{-1}$ and r/ω is apparent for the Delaware, whose geometry and tidal properties are particularly well constrained by data. From equation (3.35b), one can solve for r/ω , plug in observed values from Table 3.1, and get $r/\omega \approx 1.24$. This is quite close to our previously observed value of $(kL_w)^{-1} \approx 1.45$.

Using the identity $\exp(i\phi) = \cos \phi + i \sin \phi$, the phase of velocity relative to elevation is seen from equation (3.34a) to be

$$\phi = -\arctan\left(\frac{L_w^{-1}}{k}\right) = -\arctan\left(\frac{r}{\omega}\right). \quad (3.37)$$

Thus, as convergence and friction increase in equilibrium estuary cases [and $(kL_w)^{-1}$ and r/ω increase], the relative phase goes to 90° , as in Section 3.6. As convergence and friction decrease [and $(kL_w)^{-1}$ and r/ω go to zero], the relative phase goes to 0° , as in Section 3.7. Figure 3.10 displays observed values of the phase of velocity relative to elevation as a function of $(kL_w)^{-1}$ along several real estuaries with varying degrees of along-channel convergence. Figure 3.10 demonstrates that equation (3.37) holds reasonably well, even locally as the convergence rate changes along-channel.

By taking the absolute value of equation (3.34a), it follows from continuity that the amplitude of tidal velocity is

$$U = \frac{\omega b}{hkw[1 + (kL_w)^{-2}]^{1/2}}, \quad (3.38)$$

which reduces to equations (3.16c) and (3.21c) for the conditions in Section 3.6 [$(kL_w)^{-1} \gg 1$] and in Section 3.7 [$(kL_w)^{-1} \ll 1$], respectively.

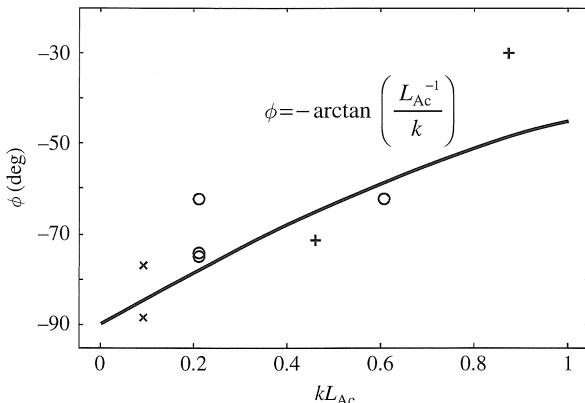


Figure 3.10. Observed phase of tidal velocity relative to tidal elevation as a function of kL_{Ac} along the Tamar (\times), Thames (\circ), and Delaware (+) (modified from Friedrichs and Aubrey, 1994). $L_{Ac} \approx L_w$ is the along-channel e-folding length for the convergence of channel cross-sectional area. For this analysis, Friedrichs and Aubrey (1994) defined L_{Ac} based on an exponential fit to $A_c(x)$ in the local vicinity of the tidal observations. Also shown is the analytical prediction given by equation (3.37).

3.11. Tides in long, non-equilibrium estuaries

We now allow tidal amplitude to change with distance along-channel and assume a solution that is the real part of:

$$\begin{aligned}\eta(x, t) &= a_0 \exp(x/L_a) \exp [i(\omega t - kx)], \\ u(x, t) &= U_0 \exp(x/L_a) \exp [i(\omega t - kx - \phi)]\end{aligned}\quad (3.39a,b)$$

[although we still require nearly constant depth, $a/h \ll 1$, $\Delta b/b \ll 1$, and $b \sim w \sim \exp(-x/L_w)$]. Following a derivation analogous to that used in Section 3.10, equation (3.39) can be substituted into ~~equation (3.2)~~, and one can separately balance the real and imaginary parts to derive: **e� . (3.2) & (3.17)**

$$\frac{c^2}{(ghw/b)} = \frac{\omega}{r} \left(\frac{L_w^{-1}}{k} - \frac{2L_a^{-1}}{k} \right) \quad \text{and} \quad \frac{c^2}{(ghw/b)} = 1 + \frac{L_w^{-1}}{k} \frac{L_a^{-1}}{k} - \left(\frac{L_a^{-1}}{k} \right)^2. \quad (3.40a,b)$$

Eliminating c from equation (3.40) yields:

$$\frac{L_a^{-1}}{k} = \frac{\omega}{r} + \frac{1}{2kL_w} - \left(\frac{\omega^2}{r^2} + 1 + \frac{1}{4(kL_w)^2} \right)^{1/2}. \quad (3.41)$$

The real and imaginary parts of continuity can be combined to show:

$$\phi = -\arctan \left(\frac{(L_w)^{-1}}{k} - \frac{(L_a)^{-1}}{k} \right). \quad (3.42)$$

And from momentum it follows that:

$$U_0 = gh \frac{a_0}{h} \frac{k}{\omega} \left| \frac{i - (kL_a)^{-1}}{i + r/\omega} \right|. \quad (3.43)$$

Similar solutions for this generalized non-equilibrium case are provided by Savenije *et al.* (2008). Several simpler asymptotes follow from equations (3.40)–(3.42). As $(kL_a)^{-1} \rightarrow 0$, equations (3.40) and (3.42) reduce to equations (3.35) and (3.37), which is the equilibrium solution (as in Sections 3.6, 3.7 and 3.10). As $(kL_w)^{-1} \rightarrow 0$ and $r/\omega \rightarrow \infty$, we have the case of a long, straight channel with strong friction, as in Section 3.8, and equations (3.41) and (3.42) reduce to $(kL_a)^{-1} = -1$ and $\phi = -45^\circ$.

We can also consider arbitrary channel convergence with zero friction ($r/\omega \rightarrow 0$) as long as we require $L_a \rightarrow 2L_w$ [otherwise c becomes undefined in equation (3.40a)]. Then we have

$$\frac{L_a^{-1}}{k} = \frac{L_w^{-1}}{2k}, \quad \frac{c^2}{(ghw/b)} = 1 + \left(\frac{L_w^{-1}}{2k} \right)^2, \quad \text{and} \quad \phi = -\arctan \left(\frac{L_w^{-1}}{2k} \right). \quad (3.44a-c)$$

Keeping in mind the definitions $a \sim \exp(x/L_a)$ and $w \sim \exp(-x/L_w)$, the frictionless asymptote in equation (3.44a) gives $a \sim w^{-1/2}$, which is the classic Green's Law solution for constant depth. The strong increase in tidal range toward the head of the Gulf of Maine, for example, results from strong convergence in combination with relatively low friction. We also see from equation (3.44) that in the absence of friction, strong convergence causes $c \rightarrow \infty$ and $\phi \rightarrow -90^\circ$ (cf. Jay, 1991).

For a long, constant-width channel with unconstrained friction [i.e., $(kL_w)^{-1} \rightarrow 0$ with arbitrary r/ω , cf. Ippen and Harleman, 1966], equation (3.40) and (3.41) reduce to

$$\frac{L_a^{-1}}{k} = \frac{\omega}{r} - \left(\frac{\omega^2}{r^2} + 1 \right)^{1/2} \quad \text{and} \quad \frac{c^2}{(ghw/b)} = 1 - \left(\frac{L_a^{-1}}{k} \right)^2. \quad (3.45a,b)$$

In other words, if a channel is non-convergent, long and frictional, equation (3.45a) indicates that L_a^{-1} is always negative (i.e., tidal amplitude always decreases landward), and equation (3.45b) tells us that wave speed is always less than the equilibrium value. For equation (3.45) [and for equations (3.40) and (3.41)], one can explicitly solve for wave speed by solving first for $(kL_a)^{-1}$.

For a long, constant-width channel, the momentum-based velocity amplitude solution given by equation (3.43) remains the same, but the relative phase solution in equation (3.42) reduces to

$$\phi = \arctan \left(\frac{L_a^{-1}}{k} \right). \quad (3.46)$$

Thus the phase of velocity relative to elevation in a long, constant-width channel ranges between $\phi = 0^\circ$ for no friction [i.e., $(kL_a)^{-1} \rightarrow 0$, equivalent to Section 3.7] and $\phi = -45^\circ$ for high friction [i.e., $(kL_a)^{-1} \rightarrow -\infty$, equivalent to Section 3.8].

3.12. Tides in long, near-equilibrium estuaries

For the observationally common case (cf. Prandle, 2004) where along-channel changes in tidal amplitude are small relative to the effects of channel convergence and along-channel tidal phase i.e., $(kL_a)^{-1} < (kL_w)^{-1} = O(1)$, a logical next approximation is to keep terms that are $O(kL_a)^{-1}$, but drop terms of relative size $O(kL_a)^{-2}$. Then the far right-hand term in equations (3.40b) can be neglected, and equation (3.40b) becomes (cf. Friedrichs and Aubrey, 1994):

$$\frac{c^2}{(ghw/b)} = 1 + \frac{L_w^{-1}}{k} \frac{L_a^{-1}}{k}, \quad (3.47)$$

while the equation for ϕ remains the same as equation (3.42). Combining equation (3.47) and equation (3.40a) then yields

$$\frac{L_a^{-1}}{k} = \frac{(kL_w)^{-1} - (r/\omega)}{2 + (r/\omega)(kL_w)^{-1}}. \quad (3.48)$$

By working backward from equation (3.47), it can further be shown that this approximation is equivalent to dropping the $\partial U / \partial x$ term on the r.h.s. of continuity while keeping the $\partial a / \partial x$ term within the pressure gradient in momentum.

Equation (3.48) highlights the competing roles of channel convergence $(kL_w)^{-1}$ and friction (r/ω) . If convergence overcomes friction, i.e., $(kL_w)^{-1} > (r/\omega)$, then $(kL_a)^{-1}$ is positive, and tidal amplitude increases as one moves landward. Such an estuary is termed hypersynchronous (Nichols and Biggs, 1985). If friction overcomes convergence, i.e., $(r/\omega) > (kL_w)^{-1}$, then $(kL_a)^{-1}$ is negative, the amplitude decreases landward, and the estuary is hyposynchronous. Equation (3.47) highlights the association between amplitude change and wave speed. If tidal amplitude grows as one moves landward, the tidal phase speed is greater than the classic “friction-less” value of $(ghw/b)^{1/2}$, but if amplitude decays landward, the phase speed is less than $(ghw/b)^{1/2}$. The tipping point for landward growth or decay of tidal amplitude then becomes the following value of the along-channel convergence length scale:

$$L_w = \frac{\omega}{rk} = \frac{(ghw/b)^{1/2}}{r} \quad (3.49)$$

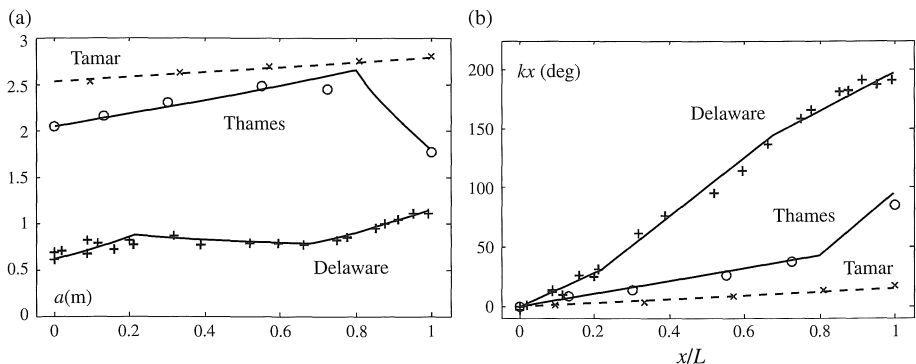


Figure 3.11. Along-estuary variation in (a) tidal elevation amplitude and (b) tidal phase with results of equations (3.39), (3.47), and (3.48) superimposed on segmented, exponentially convergent channels (\times Tamar, \circ Thames, $+$ Delaware). Adapted from Friedrichs and Aubrey (1994).

(cf. Le Floch, 1961). If the e-folding length of channel convergence is less than c/r , then amplitude grows, but if the e-folding length is greater than c/r , amplitude decays.

Equations (3.39), (3.47) and (3.48) are consistent with observed changes in tidal amplitude and phase speed along near-equilibrium estuaries (Fig. 3.11). Based on least-squares exponential fits to along-channel variations in channel geometry, Friedrichs and Aubrey (1994) divided up the Delaware into three segments, divided the Thames into two segments, and represented the Tamar with one segment. As predicted by equation (3.48), observed increases and decreases in tidal amplitude as one moves along-channel are consistent with inferred local values of $(kL_w)^{-1}$ and (r/ω) . Furthermore, in the systems fit with more than one segment, changes in the sign of $(kL_a)^{-1}$ from one segment to the next agree with changes in c as predicted by equation (3.47) (Fig. 3.11). Where the next up-estuary segment is marked by a switch from positive to negative $(kL_a)^{-1}$, the change in $(kL_a)^{-1}$ is accompanied by a decrease in c (i.e., an increase in the slope of kx); likewise, a switch from negative to positive $(kL_a)^{-1}$ causes c to increase once more.

3.13. Tides in intermediate-length estuaries

An intermediate-length tidal estuary is defined as one where the inner end of the channel has a major impact on the tide through a notable fraction of the estuary, yet the estuary is too long to apply the short-channel solution (i.e., it is *not* true that both $kL \ll 1$ and $L/L_a \ll 1$). Examples of real tidal embayments that are reasonably represented by this approximation include Long Island Sound, USA (Swanson, 1976) and Gulf St. Vincent, Australia (Bowers and Lennon, 1990). Since

intermediate-length, approximately rectangular, “dead-end” channels are not morphodynamically stable, they tend to form within relict features such as tectonic basins or submerged glacial topography rather than within classical river valley estuaries.

The effect of a barrier at the head of a channel can manifest itself away from the inner wall via a reflected wave that can be included in the expression for tidal elevation:

$$\eta(x, t) = a_I(x) \cos(\omega t - k_I x) + a_R(x) \cos(\omega t + k_R x - \phi_R). \quad (3.50)$$

In equation (3.50), a_I and a_R represent the potentially x -dependent amplitudes of the incident and reflected components, k_I and k_R are the potentially distinct incident and reflected wave numbers, and ϕ_R is the relative phase of the reflected wave. It is important to note that where the reflected wave is significant, the observed wave number, based on the observed phase speed, will be different from k_I and k_R . Up until this point in this chapter, k always represented the directly observed wave number (k_{obs}) that can be observationally derived from the observed variation in tidal phase along the estuary.

The difference between k_{obs} and k_I in the context of an intermediate-length, nearly constant-width channel is demonstrated well by the example of Gulf St. Vincent (Bowers and Lennon, 1990). The observed phase speed, ω/k_{obs} , of ~ 60 m/s over the inner 120 km of the Gulf (Fig. 3.12) is much greater than the theoretical incident

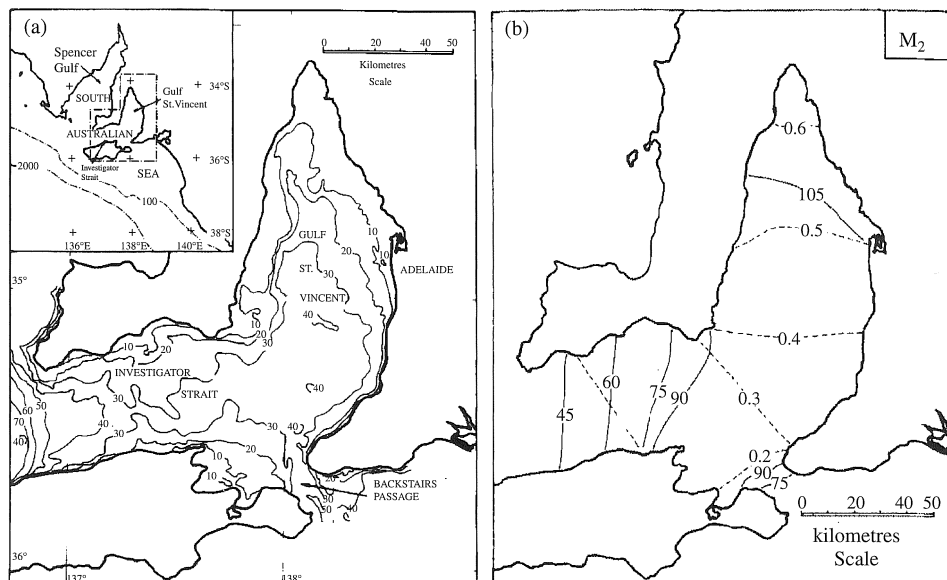


Figure 3.12. (a) Location map of the Investigator Strait – Gulf of St Vincent system, with depth contours in meters. (b) Observed amplitude in meters (dashed line) and phase in degrees (solid line) of M_2 tidal elevation. From Bowers and Lennon (1990).

wave speed, $\omega/k_I \approx (gh)^{1/2}$, of ~ 16 m/s. Also, the doubling of the observed tidal amplitude over this distance indicates that L/L_{a_obs} is not much less than one, so the short-channel solution from Section 3.5 is not applicable.

The region near the channel head where a reflected wave is important is delimited by the point at which a_R/a_I becomes small, or about $a_R/a_I \approx 1/e$ for the leading-order accuracy with which this chapter is concerned. For the case of a non-convergent estuary with an abrupt reflecting wall, we have $k_I = k_R$, and both a_I and a_R will decay equally with propagation distance. It follows that a reflected wave should be included for distances from the head wall less than about $|L_a|/2$, where $|L_a|$ is the absolute value of L_a as predicted by equation (3.45a), not the observed value (L_{a_obs}) discussed in the previous paragraph. Within the region where the reflected wave is important, the total wave solution can be calculated by using equation (3.45) to determine L_a and c for the incident and reflected components separately, adding the two components together, and choosing ϕ_R via continuity to satisfy no volume flux at $x = L$.

For the case of an equilibrium or near-equilibrium estuary, the rate at which friction reduces tidal amplitude $(L_{a_frict})^{-1}$ can be estimated from equation (3.44a) as equal to the spatial rate of change that would have occurred without friction, i.e., $|(L_{a_frict})^{-1}| \approx (L_w^{-1})/2$. Once the wave has been reflected, the effect of channel divergence alone also follows from equation (3.44a) as $|(L_{a_diverg})^{-1}| \approx (L_w^{-1})/2$. The combined effect of both friction and divergence on the reflected wave is then approximately $|(L_{a_frict})^{-1} + (L_{a_diverg})^{-1}| \approx L_w^{-1}$. Thus, in a nearly equilibrium estuary, the reflected wave can be neglected at distances greater than about L_w from the inner end of the channel.

3.14. Compact solutions for tides in intermediate-length, non-convergent estuaries

There are two cases for intermediate-length, straight estuaries where the incident and reflected waves in equation (3.50) can be combined to form particularly compact expressions, namely with very low friction ($r/\omega \rightarrow 0$) and with very high friction ($r/\omega \rightarrow \infty$). The following, very low friction solution for η can be found by letting $a_I = a_R = a_0$ in equation (3.50), setting $\phi_R = 0$ at $x = L$, and employing trigonometric identities. The solution for u then follows directly from continuity:

$$\begin{aligned}\eta(x, t) &= a_0 \frac{\cos k(L-x)}{\cos kL} \cos \omega t, \\ u(x, t) &= -\frac{a_0}{h} \left(\frac{ghb}{w} \right)^{1/2} \frac{\sin k(L-x)}{\cos kL} \sin \omega t.\end{aligned}\tag{3.51a,b}$$

In equation (3.51), k is not the observed wave number based on observed phase propagation, but rather the equivalent k for an infinite, straight, frictionless channel as in Section 3.7. The solution in equation (3.51) can lead to the classical case of “quarter wave resonance”. This name arises from the fact that the denominator of equation (3.51) becomes undefined, and a and $U \rightarrow \infty$ when the estuary length $L = (2\pi/k)/4 = \lambda/4$, where λ is the length of the associated frictionless progressive wavelength. (Of course in practice, tidal amplitude would stop growing because of enhanced frictional damping.) For $L > \lambda/4$, one or more tidal nodes appear within the estuary, where tidal amplitude is zero but velocity is at a maximum. For short systems ($kL \ll 1$), equation (3.51) reduces to the linearized tidal pumping solution given by equation (3.14).

The very high friction case yields the real parts of:

$$\begin{aligned}\eta(x, t) &= a_0 \frac{\cosh k'(L-x)}{\cosh k'L} \exp(i\omega t) , \\ u(x, t) &= U_0 \frac{\sinh k'(L-x)}{\cosh k'L} \exp[i(\omega t + \pi/4)] ,\end{aligned}\quad (3.52a,b)$$

where $k' = (1+i) k$ (Friedrichs and Madsen, 1992), and U_0 is given by equation (3.26b). In equation (3.52) k is once more not the observed wavenumber based on observed phase propagation, but this time the equivalent k for a long, constant-width, frictionally dominated channel as in Section 3.8. For long systems ($kL \gg 1$), equation (3.52) reduces to equations (3.25) and (3.26), while for short systems ($kL \ll 1$), equation (3.52) reduces to equation (3.14). Friedrichs and Madsen (1992) showed that equation (3.52a) provides a useful approximation for the propagation of tidal elevation in many shallow estuaries and channelized tidal embayments. However, the quantitative utility of equation (3.52b) for predicting spatial variations in the amplitude of tidal velocity is limited by the constant channel width assumption.

3.15. Discussion and conclusions

This chapter has laid out a methodology by which widely available observations of estuary geometry and along-channel variations in tidal amplitude and phase (e.g., the e-folding length scales of L_w , L_U , L_a , and L_h , and the wave number k) can be used to scale the governing equations of continuity and conservation of mass for barotropic tides in channelized estuaries. The goal for each relevant estuarine scenario was to eliminate as many secondary terms as possible and identify the simplest physically insightful and reasonably realistic governing balances that adequately describe the problem. Table 3.3 summarizes the properties of the solutions discussed in this chapter (other than those that explicitly involve reflected

Table 3.3 Properties of linearized asymptotic solutions for estuarine tides discussed in this chapter. Except for the short channel solution, all cases assume $\eta \approx a_0 \exp(x/L_a) \cos(\omega t - kx)$, $u \approx U_0 \exp(x/L_a) \cos(\omega t - kx - \phi)$, $w \sim b \sim \exp(-x/L_w)$, $a/h \ll 1$, $\Delta b/b \ll 1$, and k and/or $L_w^{-1} \gg L_h^{-1}$. See text for discussion of cases involving reflected waves

Case	Additional key assumptions	Remaining r.h.s. terms in continuity	Remaining momentum terms	Spatial rate of change in tidal elevation amplitude relative to change in phase	Phase speed, c	Velocity relative phase, ϕ	Tidal velocity amplitude, U
(i) Short	$\frac{L}{k^{-1}} \ll 1, \frac{L}{L_a} \ll 1$	$\frac{\partial w}{\partial x}, \frac{\partial U}{\partial x}$	None	$\frac{L_a^{-1}}{k} = 0$	$c = \infty$	$\phi = -90^\circ$	$U(x) = \frac{a_0 \omega A_b(x)}{A_c(x)}$
(ii) Long, shallow, funnel-shaped	$\frac{L_w^{-1}}{k} \gg 1, \frac{L_U^{-1}}{L_w^{-1}} \ll 1$	$\frac{\partial w}{\partial x}$	$\frac{\partial(kx)}{\partial x}, ru$	$\frac{L_a^{-1}}{k} = 0$	$c = \frac{ghwL_w^{-1}}{rb}$	$\phi = -90^\circ$	$U_0 = \frac{a_0 \omega b}{h L_w^{-1} w}$
(iii) Long, deep, non-convergent	$\frac{L_w^{-1}}{k} \ll 1, \frac{L_U^{-1}}{k} \ll 1$	$\frac{\partial(kx)}{\partial x}$	$\frac{\partial u}{\partial t}, \frac{\partial(kx)}{\partial x}$	$\frac{L_a^{-1}}{k} = -1$	$c = \left(\frac{ghw}{b}\right)^{1/2}$	$\phi = 0^\circ$	$U_0 = \frac{a_0 \omega b}{hk w}$
(iv) Long, shallow, non-convergent	$\frac{L_w^{-1}}{k} \ll 1, \frac{r}{\omega} \gg 1$	$\frac{\partial(kx)}{\partial x}, \frac{\partial U}{\partial x}$	$\frac{\partial a}{\partial x}, \frac{\partial(kx)}{\partial x}, ru$	$\frac{L_a^{-1}}{k} = 0$	$c = \left(\frac{2\omega ghw}{rb}\right)^{1/2}$	$\phi = -45^\circ$	$U_0 = \frac{a_0}{h} \left(\frac{aghb}{rw}\right)^{1/2}$
(v) Long, intermediate-depth, equilibrium	$\frac{L_w^{-1}}{k} = O(1), \frac{L_U^{-1}}{k} \ll 1$	$\frac{\partial w}{\partial x}, \frac{\partial(kx)}{\partial x}$	$\frac{\partial u}{\partial t}, \frac{\partial(kx)}{\partial x}, ru$	$\frac{L_a^{-1}}{k} = 0$ $\left(\frac{r}{\omega} = \frac{L_w^{-1}}{k}\right)$	$c = \frac{ghwL_w^{-1}}{rb} = \left(\frac{ghw}{b}\right)^{1/2}$ $\phi = -\arctan\left(\frac{L_w^{-1}}{k}\right)$ $(\phi = -90^\circ \text{ to } 0^\circ)$		$U_0 = \frac{a_0 \omega b}{hk w [1 + (k L_w)^{-2}]^{1/2}}$
(vi) Long, intermediate-depth, non-convergent	$\frac{L_w^{-1}}{k} \ll 1, \frac{r}{\omega} = O(1)$	$\frac{\partial(kx)}{\partial x}, \frac{\partial U}{\partial x}$	$\frac{\partial u}{\partial t}, \frac{\partial a}{\partial x}, \frac{\partial(kx)}{\partial x}, ru$	$\frac{L_a^{-1}}{k} = \frac{\omega}{r} - \left(\frac{\omega^2}{r^2} + 1\right)^{1/2}$ $(-1 \leq (k L_a)^{-1} \leq 0)$	$\frac{c^2}{(ghw/b)} = 1 - \left(\frac{L_a^{-1}}{k}\right)^2$	$\phi = \arctan\left(\frac{L_a^{-1}}{k}\right)$ $(\phi = -45^\circ \text{ to } 0^\circ)$	$U_O = \frac{a_0 kgh}{h \omega} \left \frac{i - (k L_a)^{-1}}{i + r/\omega} \right $

(vii) Long, deep, funnel-shaped	$\frac{L_w^{-1}}{k} = O(1), \frac{r}{\omega} \ll 1$	$\frac{\partial w}{\partial x}, \frac{\partial(kx)}{\partial x}, \frac{\partial U}{\partial x}$	$\frac{\partial u}{\partial t}, \frac{\partial a}{\partial x}, \frac{\partial(kx)}{\partial x}$	$\frac{L_a^{-1}}{k} = \frac{L_w^{-1}}{2k}$	$\frac{c^2}{(ghw/b)} = 1 + \left(\frac{L_w^{-1}}{2k}\right)^2$	$\phi = -\arctan\left(\frac{L_w^{-1}}{2k}\right)$ ($\phi = -90^\circ$ to 0°)	$U_0 = \frac{a_0 k g h}{h \omega}$ $[1 - (k L_a)^{-2}]^{1/2}$
(viii) Long, intermediate- depth, near equilibrium	$(k L_w)^{-1} = O(1)$ $(k L_U)^{-1} < (k L_w)^{-1}$ Drop terms $O(k L_U)^{-2}$	$\frac{\partial w}{\partial x}, \frac{\partial(kx)}{\partial x}$	$\frac{\partial u}{\partial t}, \frac{\partial a}{\partial x}, \frac{\partial(kx)}{\partial x}, ru$	$\frac{L_a^{-1}}{k} = \frac{(k L_w)^{-1} - (r/\omega)}{2 + (r/\omega)(k L_w)^{-1}}$ ($-O(1) < (k L_a)^{-1} < O(1)$)	$\frac{c^2}{(ghw/b)} = 1 + \frac{L_w^{-1} L_a^{-1}}{k^2}$	$\phi = -\arctan\left(\frac{L_w^{-1}}{k} - \frac{L_a^{-1}}{k}\right)$ ($\phi = -90^\circ$ to 0°)	$U_0 = \frac{a_0 k g h}{h \omega} \left \frac{i - (k L_a)^{-1}}{i + r/\omega} \right $
(ix) Long, intermediate- depth, non- equilibrium	$(k L_w)^{-1} = O(1)$ $r/\omega = O(1)$ $L_w/L_a = O(1)$	$\frac{\partial w}{\partial x}, \frac{\partial(kx)}{\partial x}, \frac{\partial U}{\partial x}$	$\frac{\partial u}{\partial t}, \frac{\partial a}{\partial x}, \frac{\partial(kx)}{\partial x}, ru$	$\frac{L_a^{-1}}{k} = \frac{\omega}{r} + \frac{L_w^{-1}}{2k}$ $- \left(\frac{\omega^2}{r^2} + 1 + \left(\frac{L_w^{-1}}{2k} \right)^2 \right)^{1/2}$	$\frac{c^2}{(ghw/b)} = 1 + \frac{L_w^{-1} L_a^{-1}}{k^2}$ $- \left(\frac{L_a^{-1}}{k} \right)^2$	$\phi = -\arctan\left(\frac{L_w^{-1}}{k} - \frac{L_a^{-1}}{k}\right)$ ($\phi = -90^\circ$ to 0°)	$U_0 = \frac{a_0 k g h}{h \omega} \left \frac{i - (k L_a)^{-1}}{i + r/\omega} \right $

waves or tidal asymmetries). The scenarios are arranged in Table 3.3 in order of the increasing number of terms retained in each case in the associated continuity and momentum equations. A theme common to all cases is the potential role of the full estuary width, b (including tidal storage in marsh, flats, shoals and tributaries), relative to the width of the momentum transporting channel, w , such that a small value of w/b tends to slow the speed of tidal phase propagation.

The first two cases in Table 3.3 [(i) short estuaries and (ii) shallow, funnel-shaped estuaries] involve scenarios where simple solutions for the amplitude of tidal velocity as a function of external parameters follow directly from the continuity equation without the need to consider momentum. In each of these cases, spatial gradients in volume flux are dominated by the system's abrupt morphology, namely limited channel length ($\sim L^{-1}$) in very short estuaries and rapid width convergence ($\sim L_w^{-1}$) in shallow, funnel-shaped systems. Another property common to cases (i) and (ii) is a "standing wave" relationship between velocity and elevation, such that tidal velocity leads elevation by 90°. Yet in neither case is a reflected wave explicitly present. In case (ii), the tidal waveform is in fact clearly "progressive" in that it propagates unidirectionally up-estuary. This highlights the potential confusion that may result if an estuary as a whole is characterized as having a "standing" or "progressive" wave character, based only on the phase relationship between velocity and elevation.

Cases (ii), (iii), (v), and (viii) in Table 3.3 represent a spectrum of naturally common "equilibrium" to "near-equilibrium" tidal estuaries characterized by small along-channel changes in the amplitude of tidal velocity. In equilibrium to near-equilibrium estuaries, $\partial U/\partial x$ is negligible relative to other sources of flux gradients in the continuity equation. Relatively constant $U(x)$ is favored by negative morphodynamic feedback: if the estuary channel were randomly perturbed to produce highly variable depth, then the locally shallower, constricted, and thus higher-velocity areas would tend to scour, while deeper and lower-velocity areas would tend to accrete, favoring an evolution back toward uniform $U(x)$. The shallow, funnel-shaped estuary [case (ii)] and the deep, constant-width estuary [case (iii)] represent the two extremes where observed channel shape and $\partial U/\partial x \approx 0$ together necessitate the simplest possible dynamic balances: friction (ru) vs the phase-induced pressure gradient [$\partial(kx)/\partial x$] in the first scenario, and $\partial u/\partial t$ vs $\partial(kx)/\partial x$ in the second. In neither case is it necessary to know the size of the friction term a priori in order to infer its relative importance.

Unlike cases (ii) and (iii), cases (v) and (viii) allow along-channel gradients in width and velocity phase to simultaneously contribute to continuity [$(kL_w)^{-1} \approx O(1)$]. Since $\partial U/\partial x$ is still small, it must follow that friction and acceleration can simultaneously contribute to momentum [$r/\omega \approx O(1)$]. In fact, these two cases indicate that for $\partial U/\partial x \approx 0$ in general, it must follow that $(kL_w)^{-1} \approx r/\omega$. This

equality leads to the somewhat surprising result that the tidal phase speed, c , in all equilibrium estuaries is equal to the frictionless value for a rectangular channel of the same depth, regardless of the actual size of the friction term. The equilibrium case highlights a balance between the competing roles of channel convergence [$(kL_w)^{-1}$], which causes amplitude to increase, and friction (r/ω), which causes amplitude to decay. In near-equilibrium estuaries, if friction overcomes convergence, i.e., $(r/\omega) > (kL_w)^{-1}$, then tidal amplitude decreases gradually along the estuary [$(kL_a)^{-1} < 0$], and c is slightly less than its frictionless value. If convergence overcomes friction, i.e., $(kL_w)^{-1} > (r/\omega)$, then tidal amplitude increases up-estuary [$(kL_a)^{-1} > 0$], and c is slightly greater than its frictionless value. The rate of channel convergence also determines the phase relationship (ϕ) between velocity and elevation, such that $\phi \approx -\arctan((kL_w)^{-1})$. Strong convergence pushes ϕ toward -90° , whereas weak convergence pushes ϕ toward 0° .

Cases (iii), (iv), and (vi) in Table 3.3 represent classic long, rectangular channel scenarios with weak, strong and intermediate friction, respectively. If friction is present without a reflected wave or channel convergence, then tidal amplitude always decreases with distance, and the tidal phase speed is always less than its frictionless value. As r/ω increases, c decreases, and the rate of amplitude decay with distance (L_a^{-1}) increases. However, with constant width, the spatial rate of amplitude decay is limited by the tidal wave number, i.e., $L_a^{-1} \leq k$. Weak friction pushes ϕ toward 0° , whereas strong friction pushes ϕ toward 90° .

Cases (iv), (vi), (vii), and (ix) are all non-equilibrium estuaries characterized by significant changes in tidal velocity amplitude with distance along-channel such that $\partial U / \partial x$ is a leading-order term in the continuity equation. For cases involving long, straight channels with friction [cases (iv) and (vi)], tidal amplitude must decrease with distance up-estuary. Case (vii) is a funnel-shaped estuary without friction, such that channel convergence (or divergence) increases (or decreases) amplitude with distance following Green's Law. Finally, case (ix) is the most general (and most complicated) case, which allows for an arbitrarily large or small increase or decrease in tidal amplitude with distance as a function of convergence, divergence, and/or friction. All the other long-channel scenarios considered in this chapter could alternately be derived by applying simplifying asymptotes to this general case.

There exist some cases (not included in Table 3.3) where a head wall in a real estuary or embayment affects the tides over a notable fraction of the system such that the dynamics are best understood by explicitly including a reflected wave component (see Sections 3.13 and 3.14 of the text). The fraction of the inner estuary affected by a reflected wave can easily be estimated for a constant-width or equilibrium/near-equilibrium estuary. In addition, compact, whole-estuary solutions are available for dead-end, non-covergent channels with very high or very low friction. When a significant reflected wave is present in a real estuary, however, it is

important to recognize the differences between the length scales associated with along-channel changes in (a) the observed tidal phase and amplitude, (b) the theoretical incident wave, and (c) the theoretical reflected wave, all three of which may have distinct values for effective k and L_a^{-1} .

Finally, short and shallow channel solutions (see Sections 3.5 and 3.9 of the text) provide insights into how temporal variations in estuary depth and width produce tidal asymmetries in velocity and elevation. Tidal variations in estuary width act to distort the tide in two ways. First, a much greater total estuary width around high water (due to extensive intertidal flats and/or marsh, i.e., large $\Delta b/b$) causes more water to move in and out of the estuary around high tide than around low tide. This leads to a pulse of higher flood and ebb velocities around high water and a shortened period of high-water slack. Second, a much wider estuary around high water also slows the along-estuary propagation speed of high tide (c_{HT}) relative to low tide (c_{LT}). With $c_{HT} < c_{LT}$, up-estuary propagation of low water partially “catches up” with the previous high water, shortening the duration of the falling tide and, via continuity, favoring ebb-dominance. Conversely, a much deeper estuary around high water (due to a large value of a/h) reduces the magnitude of velocity around high tide because the cross-sectional area of the channel is larger then, and the duration of high-water slack is therefore increased. Second, a deeper estuary around high tide increases c_{HT} relative to c_{LT} . With $c_{HT} > c_{LT}$, high tide partially catches up with the previous low tide. The tide then rises more quickly, and flood dominance is favored.

Acknowledgments

Work on this chapter was supported in part by National Science Foundation Grant OCE-0536572. This is contribution no. 3005 from the Virginia Institute of Marine Science, College of William and Mary.

References

- Boon, J. D. (1975) Tidal discharge asymmetry in a salt marsh drainage system. *Limnol. Oceanogr.* **20**, 71–80.
- Bowers, D. G. and G. W. Lennon (1990) Tidal procession in a near-resonant system – a case study from South Australia. *Est. Coast. Shelf Sci.* **30**, 17–34.
- Carter, H. H. and D. W. Pritchard (1988) Oceanography of Chesapeake Bay. In B. Kjerfve (ed.), *Hydrodynamics of Estuaries, 2. Estuarine Case Studies*. CRC Press, Boca Raton, Florida.
- Friedrichs, C. T. (1995) Stability shear stress and equilibrium cross-sectional geometry of sheltered tidal channels. *J. Coastal Res.* **11**, 1062–1074.
- Friedrichs, C. T. and D. G. Aubrey (1988) Non-linear tidal distortion in shallow well-mixed estuaries: a synthesis. *Est. Coast. Shelf Sci.* **27**, 521–545.

- Friedrichs, C. T. and D. G. Aubrey (1994) Tidal propagation in strongly convergent channels. *J. Geophys. Res.* **99**, 3321–3336.
- Friedrichs, C. T. and O. S. Madsen (1992) Nonlinear diffusion of the tidal signal in frictionally-dominated embayments. *J. Geophys. Res.* **97**, 5637–5650.
- Friedrichs, C. T., B. A. Armbrust and H. E. de Swart (1998) Hydrodynamics and equilibrium sediment dynamics of shallow, funnel-shaped tidal estuaries. In J. Dronkers and M. Scheffers (eds), *Physics of Estuaries and Coastal Seas*. Balkema Press, Rotterdam, pp. 315–328.
- Hunt, J. N. (1964) Tidal oscillations in estuaries. *Geophys. J. Roy. Astron. Soc.* **8**, 440–455.
- Ippen, A. T. and D. R. F. Harleman (1966) Tidal dynamics in estuaries. In A. P. Ippen (ed.), *Estuary and Coastline Hydrodynamics*. McGraw-Hill, New York, pp. 493–545.
- Jay, D. A. (1991) Green's Law revisited: tidal long-wave propagation in channels with strong topography. *J. Geophys. Res.* **96**, 20,585–20,598.
- Lanzoni, S. and G. Seminara (1998) On tide propagation in convergent estuaries. *J. Geophys. Res.* **103**, 30,793–30,812.
- Le Floch, J. (1961) *Propagation de la marée dans l'estuaire de la Seine et en Seine-Maritime*. ScD thesis, University of Paris, 507 pp.
- Nichols, M. M. and R. B. Biggs (1985) Estuaries. In R. A. Davis (ed.), *Sedimentary Environments*, 2nd edn. Springer-Verlag, New York, pp. 77–186.
- NOAA (1985) *National Estuarine Inventory: Data atlas. Volume 1. Physical and Hydrologic Characteristics*. NOAA/NOS Strategic Assessment Branch, Rockville, MD, 103 pp.
- Parker, B. B. (1991) The relative importance of the various nonlinear mechanisms in a wide range of tidal interactions. In B. B. Parker (ed.), *Tidal Hydrodynamics*. John Wiley & Sons, New York, pp. 237–268.
- Pethick, J. S. (1980) Velocity surges and asymmetry in tidal channels. *Est. Coast. Mar. Sci.* **11**, 331–345.
- Prandle, D. (2003) Relationships between tidal dynamics and bathymetry in strongly convergent channels. *J. Phys. Oceanogr.* **33**, 2738–2750.
- Prandle, D. (2004) How tides and river flows determine estuarine bathymetries. *Progr. Oceanogr.* **61**, 1–26.
- Robinson, I. S., L. Warren and J. F. Longbottom (1983) Sea-level fluctuations in the Fleet, an English tidal lagoon. *Est. Coast. Shelf Sci.* **16**, 651–668.
- Savenije, H. H. G., M. Toffolon, J. Haas and J. M. Veling (2008) Analytical description of tidal dynamics in convergent estuaries. *J. Geophys. Res.* **113**, C10025, doi:10.1029/2007JC004408.
- Savenije, H. H. G. and E. J. M. Veling (2005) Relation between tidal damping and wave celerity in estuaries. *J. Geophys. Res.* **110**, C04007, doi:10.1029/2004JC002278.
- Spitz, Y. H. and J. M. Klinck (1998) Estimate of bottom and surface stress during a spring-neap tide cycle by dynamical assimilation of tide gauge observations in the Chesapeake Bay. *J. Geophys. Res.* **103**, 12,761–12,782.
- Swanson, R. L. (1976) *Tides*. Marine EcoSystems Analysis Program, MESA New York Eight Atlas Monograph 4, New York, Sea Grant Institute, Albany, NY, 44 pp.